ACS NANO
Cite This: ACS Nano 2018, 12, 368–377
www.acsnano.org

ARTICLE

Energy Dissipation in Fluid Coupled Nanoresonators: The Effect of Phonon-Fluid Coupling

Subhadeep De[†] and Narayana R. Aluru[*,†,‡]

[†]Department of Mechanical Science and Engineering and [‡]Beckman Institute for Advanced Science and Technology, University of Illinois at Urbana−Champaign, Urbana, Illinois 61801, United States

ABSTRACT: **Resonant nanomechanical systems find numerous sensing applications both in the vacuum and in the fluid environment but their performance is degraded by different dissipation mechanisms. In this work, we study dissipation mechanisms associated with high frequency axial excitation of a single-walled carbon nanotube (CNT) filled with argon, which is a representative fluid coupled resonator system. By performing molecular dynamics simulations, we identify two dissipative processes associated with the axial excitation of the resonator: (i) perturbation of the resonator phonons and their relaxation and (ii) oscillatory fluid flow developed by the resonator motion. Dissipation due to the first process, a form of "intrinsic" dissipation, is found to be governed by the Akhiezer mechanism and is verified for an empty CNT in vacuum. To estimate the dissipation due to the second process, which is the conventional "fluid" dissipation, we formulate an approach based on the response of the hydrodynamic force on the resonator. Our analysis of the coupled system reveals that phonon relaxations associated with the Akhiezer dissipation are significantly modified in the presence of fluidic interactions, which have been ignored in all previous dissipation studies of fluid-resonator systems. We show that an important consequence of this phonon-fluid interaction is inverse scaling of dissipation with density at low excitation frequencies.**

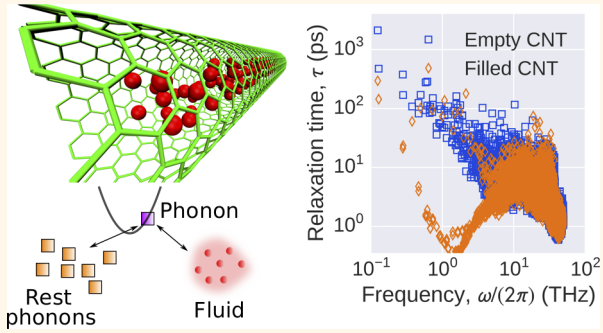

KEYWORDS: *nanoscale fluid-structure interaction, dissipation, phonons, fluid, relaxation time, molecular dynamics*

Structures with nanometer dimension have revolutionized the realm of ultrasensitive sensing and precision measurements over the past decade.[1] Sensors based on nanowires[2] and nanotubes[3,4] with unparalleled sensitivity have already been demonstrated in chemical and biological sensing applications. While in some cases, the sensing is based on the change in the electrical conductance of the nanostructure with surface adsorption of charged molecules,[5,6] a more popular approach is to utilize the resonant mechanical motion of the nanostructure.[7] In the latter case, the principle behind inertial mass detection is based on the shift in resonant frequency due to adsorption of the atomic species on the surface of the resonator.[3,8] Central to the sensitivity of these resonant nanomechanical systems is dissipation which limits the performance. For instance, a low dissipation ensures better resolution of frequency shift during mass sensing. Various nanoresonators exhibit considerably high quality factor at room temperature when operated in vacuum.[7,9−11] However, many practical applications, like real-time nanoresonator-based mass spectroscopy, demand masses of analytes to be detected from a liquid environment.[12,13] In such cases, viscous drag by the fluid medium is expected to degrade the quality factor of the resonator. The dissipation mechanisms, like thermoelastic damping (TED),[14] Akhiezer damping,[15,16] surface, and defect mediated losses,[17] are intrinsic to the material and geometry of the resonator. While intrinsic dissipation plays a major role in vacuum operating condition, fluid damping, which acts as a source of extrinsic dissipation, becomes equally important or even more dominant when the resonator is coupled with a fluid medium. High frequency nanofluidic experiments, carried out to characterize the fluid flow and dissipation due to vibrating resonators in a gas-filled chamber have revealed that the presence of "surrounding" fluid increases the dissipation of the resonator by manifolds. This, being detrimental to the resonator sensitivity, a novel strategy has been employed to measure the mass of the analytes from the liquid. Confining the liquid with bound mass in a fluidic channel "inside" the resonator surrounded by vacuum[18] has demonstrated measurements with femtogram to attogram sensitivity due to a drastic reduction in fluid dissipation.[19,20] In all these fluid coupled resonators, the key way to assess the limits of performance is to understand the individual mechanisms of energy dissipation.

Received: September 11, 2017
Accepted: December 29, 2017
Published: December 29, 2017

DOI: 10.1021/acsnano.7b06469
ACS Nano 2018, 12, 368–377

For a nanomechanical resonator operating at gigahertz frequency at room temperature and isolated in vacuum, phonon-mediated dissipation is a major source of intrinsic dissipation.[15] To explain the underlying dissipation mechanism, different theories, like TED theory[14,21] and Akhiezer theory,[16,22,23] are recently revisited and developed in the context of high frequency resonators. These dissipation mechanisms depend on different phonon properties, like phonon relaxation time, phonon Grüneisen parameter, thermal expansion coefficient, phonon group velocities, etc. The resonator, when coupled with a fluid medium and driven, develops an oscillating flow-field in the fluid. Due to the viscous nature of the fluid medium, the flow is associated with energy loss which is conventionally known as fluid dissipation (D_{flu}). Hence, in a fluid coupled resonator system, the driven resonator continuously loses energy to phonons and fluids. We denote the net dissipation of any such system by D_{sys}. Recently, the study of fluid dissipation in these systems with nanometer scale resonators drew a lot of attention. The vibration of resonators of this length-scale involves a parameter space where continuum theories, like Navier–Stokes, used to describe the oscillatory fluid dynamics break down.[24−26] An indication of this transition is the change in slope of the scaling of fluid dissipation with pressure or density of the fluid. This motivated a lot of experiments toward quantifying fluid dissipation. In most of the experimental studies, the standard way of calculating D_{flu} is to subtract the intrinsic dissipation component from D_{sys}, *i.e.*, $D_{flu}=D_{sys}-D^{v}_{int}$,[26−29] where D^{v}_{int} is the intrinsic dissipation in the structure obtained separately in near vacuum condition. This decomposition is only possible under the assumption that the processes associated with each dissipation mechanism are independent. Here, we show that, in the presence of fluid, phonon relaxation times change significantly from their values in vacuum. This, in turn, modifies the intrinsic dissipation process and hence D^{v}_{int}. We denote the modified intrinsic dissipation of the structure in the presence of fluid as D^{f}_{int} (such that $D_{sys}=D^{f}_{int}+D_{flu}$) and claim that the difference ($\Delta D_{int}=D^{f}_{int}-D^{v}_{int}$) is due to phonon-fluid coupling. It is quite challenging to quantify this difference, ΔD_{int}, experimentally and hence it is ignored. However, accounting for ΔD_{int} can be particularly important when the magnitude of D_{flu} is comparable to D^{f}_{int}. Here, we rely on extensive molecular dynamics (MD) simulations to capture the phonon-fluid coupling effect on the dissipation of a fluid coupled resonator system. By formulating each dissipation process based on their underlying mechanism, we explain the rationale behind the coupling and present the consequences of the coupling effect on net dissipation.

In this study, we consider a single-walled carbon nanotube (CNT) resonator filled with argon (Ar), both CNT and Ar equilibrated at 300 K, and study dissipation during the axial mode of vibration. The stretching under axial mode can ensure that spatial distribution of strain in the structure is nearly uniform. Under this condition, intrinsic dissipation is dominated by the Akhiezer mechanism. Thus, the simplistic setup offered by axial mode of vibration provides a scope for a detailed understanding of the phonon-fluid coupling effect. We describe different simulation setups considered for computing dissipation using nonequilibrium MD simulations. In our attempt to decompose D_{sys}, we look at the mechanisms behind intrinsic and fluid dissipation. We ascertain that the intrinsic dissipation is governed by the Akhiezer mechanism by considering an empty CNT in vacuum (no fluid). We formulate the dissipation, D^{v}_{int} in terms of the phonon parameters: relaxation time (τ), Grüneisen parameter (γ). Next, we express the fluid dissipation during axial excitation of the resonator as the work done against the hydrodynamic force. In this regard, we propose an approach based on linear response theory to formulate the fluid dissipation D_{flu}, in terms of autocorrelation of equilibrium fluctuations of an observable computed using the hydrodynamic force. We confirm this approach by considering an Ar filled CNT system with thermal motions in the CNT frozen (no phonons). We found that the magnitude of D^{v}_{int} is comparable to D_{flu} for the system considered in the present study and that any change, ΔD_{int}, due to fluid coupling becomes important. For the CNT with confined Ar, we recompute the phonon relaxation times and notice significant reduction of their values for the low frequency phonon modes. We use the modified relaxation times to calculate D^{f}_{int}. We also found that an increase in the density of Ar inside CNT strengthens the coupling between phonons and fluid. We show the consequence of the coupling on the scaling of overall dissipation with density.

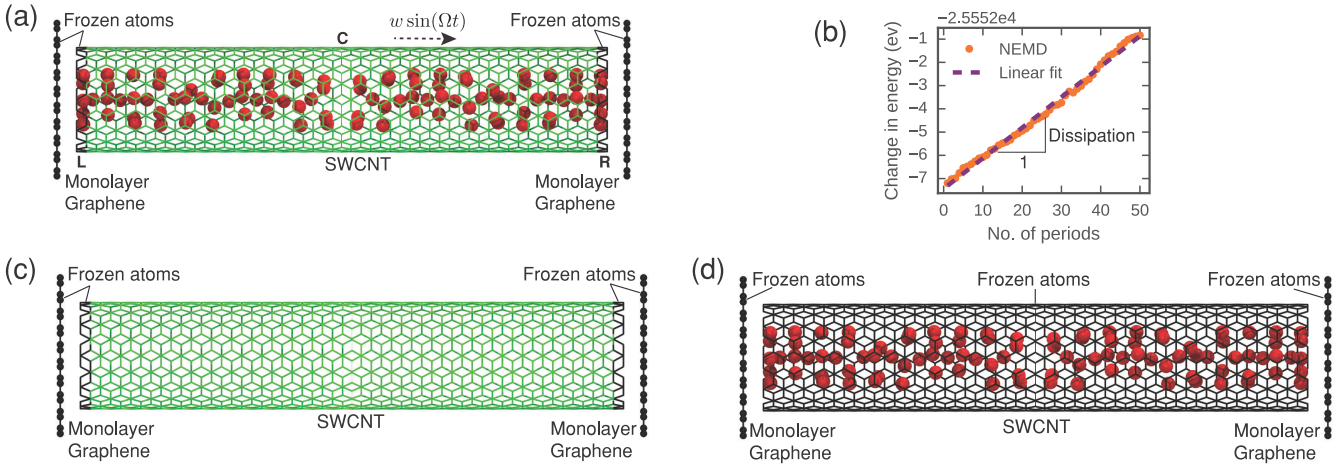

Figure 1. Simulation setup for the molecular dynamics (MD) study. (a) An argon (red spheres) filled single-walled carbon nanotube system with a sheet of monolayer graphene on each end. The carbon atoms, which are kept frozen during the simulation, are represented in black. (b) The linear growth of energy of the system with the periods of excitation during nonequilibrium molecular dynamics simulation. The rate of change in energy gives dissipation. (c) A single-walled carbon nanotube in vacuum. (d) An argon (red spheres) filled carbon nanotube system with all the carbon atoms frozen.

DOI: 10.1021/acsnano.7b06469
ACS Nano 2018, 12, 368−377

RESULTS AND DISCUSSION

Our system (sys) composed of Ar atoms inside a CNT and two graphene layers is shown in Figure 1a. The CNT and the graphene layers constitute the wall which confines the fluid, Ar. We perform nonequilibrium molecular dynamics (NEMD) simulations to compute dissipation, D_{sys} in the system under axial excitation. The dissipation can be calculated from the change in averaged total energy of the system (shown in Figure 1b) during the NEMD simulations. We present the dissipation results in terms of a nondimensional quantity called inverse quality factor, Q^{-1}, which is defined as $Q^{-1} = D/(2\pi E_{sto})$. Here, D is the energy dissipated and E_{sto} is the maximum energy stored in the system over a period of excitation. The density of Ar in the coupled system is quantified by a dimensionless number $\rho^* = N\sigma^3/\pi r^2 l$, where N is the number of Ar atoms inside the CNT, σ is the LJ diameter of Ar, r is the radius of the CNT, and l is the length of the CNT. To elucidate the different dissipation mechanisms, we consider two additional setups. The first setup (case I) is an isolated CNT at 300 K in vacuum (v) as displayed in Figure 1c. The dissipation estimated for this system is the intrinsic dissipation, D^v_{int} due to phonon perturbation and relaxation in the CNT. As the second setup (case II), we consider our original system (sys) but the thermal motions in the CNT are frozen (shown in Figure 1d). For more details on each setup and the simulation methodology, refer to the Methods Section.

Dissipation in the Coupled System. The left panel of Figure 2 shows the dissipation response of the coupled system

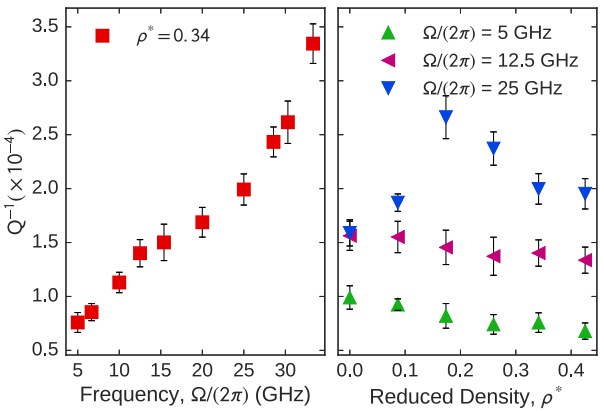

Figure 2. Left: Scaling of the inverse quality factor, Q^{-1} with frequency of periodic excitation, Ω. The reduced density, ρ^* of the confined argon is 0.34. Right: Scaling of the inverse quality factor with density of filled argon at different excitation frequencies.

(shown in Figure 1a) due to axial excitation at different frequencies for ρ^*=0.34. The particular choice of frequencies ensures that the time scale of deformation is in the order of lifetimes of the phonons, which is few picoseconds for a CNT. This is a necessary condition for the mechanical deformation to interact with the phonons and result in phonon mediated dissipation. Also, keeping the maximum excitation frequency well below the fundamental frequency of axial vibration of the CNT can simplify the strain field in the structure to be spatially uniform.[16,22] For all our cases, the strain amplitude is approximately 2%. Though dissipation increases monotonically in general, its dependence on a particular frequency is governed by the time scales associated with underlying dissipation mechanisms. The time scales depend on the self-and cross interaction between each entity constituting the system, *i.e.*, phonons and fluids. Here, we change the amount of Ar inside CNT to manipulate the phonon-fluid coupling and consequently the time scales. The right panel of Figure 2 shows the effect of scaling density, ρ^*, on dissipation of the coupled system at three different frequencies. At lower frequencies, *i.e.*, 5 and 12.5 GHz, dissipation reduces with increasing density whereas at higher frequency, *i.e.*, 25 GHz, the dissipation scales nonmonotonically. The system with $\rho^* = 0$ corresponds to the isolated CNT in vacuum. The dissipation, in this case, is due to an intrinsic damping mechanism which is mediated by phonons. With the introduction of fluid in the system, another mechanism that results in fluid damping starts playing a role. Thus, one should expect to observe an increase in dissipation with the density of Ar. An inverse scaling of dissipation with density at lower frequencies indicates that some process associated with the intrinsic dissipation mechanism is influenced by the presence of fluid. We elucidate this by analyzing the mechanism of intrinsic dissipation in detail. We also shed some light on the origin of the nonmonotonic behavior of dissipation scaling with density at higher frequencies.

To understand the intrinsic dissipation mechanism, we start with an empty CNT in vacuum (case I, shown in Figure 1c). We first describe the phonon related processes that accompany the axial excitation of the CNT and formulate an expression for intrinsic dissipation. Then, we present the results of dissipation during axial excitation estimated using NEMD simulation and validate our formulation.

Intrinsic Dissipation in Empty CNT. An empty CNT at temperature T has phonon modes of different frequencies, ω_i. In thermal equilibrium, these phonon modes share equal energy, E_i=k_BT, where k_B is the Boltzmann constant. Any strain field, ϵ generated in the structure during mechanical excitation process can perturb the energy of the phonon modes by modulating their frequencies. This thermo-mechanical coupling is quantified by the Grüneisen parameter defined as $\gamma_i = -\frac{1}{\omega_i}\frac{\partial \omega_i}{\partial \epsilon}$. The rate of frequency modulation of the phonon modes depends on the excitation frequency, Ω. When ($\Omega \ll \omega_i$), the ratio E_i/ω_i is an adiabatic invariant.[35] Using this, the rate of change of phonon energies can be related to a time-varying strain field as[36] $\frac{\partial E_i}{\partial t} = -\gamma_i E_i \dot{\epsilon}(t)$. Here, $\epsilon(t)$ can be regarded as $\epsilon_0 \sin(\Omega t)$ where ϵ_0 is the strain amplitude. Thus, the strain-field due to excitation process disturbs the equilibrium condition ($E_i = k_BT$) for phonons. The phonons try to retain the equilibrium by exchanging energies with other phonons. This process is termed as relaxation process. The phonon relaxation process is possible because different phonon modes are coupled anharmonically. Under a single relaxation time approximation,[37] the relaxation process can be expressed as $\frac{\partial E_i}{\partial t} = -\frac{E_i - \bar{E}}{\tau_i}$, where τ_i is the relaxation time of the phonon and $\bar{E}$ is the mean energy of the phonon ensemble. The energy dissipation associated with this whole process is termed as Akhiezer dissipation. The approximate analytical form for Akhiezer dissipation for a system of N phonons is given by[36]

$$D_{Akh} = \sum_{i=1}^{N} \pi k_B T \Delta\gamma_i^2 \frac{\Omega\tau_i}{1 + \Omega^2\tau_i^2}\epsilon_0^2 \quad (1)$$

Here, $\Delta\gamma_i = \gamma_i - \bar{\gamma}$ where $\bar{\gamma}$ is the mean Grüneisen parameter of the phonon ensemble and ϵ_0 is the strain amplitude. The mechanism of intrinsic dissipation described above is complete under the condition of spatially uniform strain in the structure.

DOI: 10.1021/acsnano.7b06469
ACS Nano 2018, 12, 368−377

In order to quantify the formulated Akhiezer dissipation in empty CNT, we compute γ_i and τ_i for the phonon modes using real space quasiharmonic method[38] and equilibrium molecular dynamics (EMD) trajectories.[37] The analytical form of the Tersoff potential is used to construct the stiffness matrix in the quasiharmonic method. The eigenvectors and eigenvalues of the stiffness matrix give the phonon mode shapes and the corresponding frequencies. From the trajectories, the atomic displacements and velocities of the CNT are projected on the mode shapes to get modal displacements and velocities, $\{A_i(t), \dot{A}_i(t)\}$. The modal energy fluctuation in time is calculated as $\delta E_i(t) = E_i(t) - \langle E_i \rangle$ where $E_i(t) = \frac{1}{2}\dot{A}_i^2(t) + \frac{1}{2}\omega_i^2 A_i^2(t)$ and $\langle E_i \rangle$ is the mean of $E_i(t)$ over time. Taking autocorrelation of energy fluctuations, relaxation time of each mode is calculated as[39] $\tau_i = \int_0^\infty \frac{\langle \delta E_i(0)\delta E_i(t)\rangle}{\langle \delta E_i^2 \rangle}$. Physically, this is the time taken by a phonon mode to equilibrate after a small perturbation in its energy. For the γ_i's, the stiffness matrix is first differentiated with respect to strain and its eigenvalues, λ_i are calculated. These eigenvalues are related to γ_i as $\lambda_i = -2\omega_i^2\gamma_i$. γ_i and τ_i thus calculated for the case of an empty CNT at 300 K are shown in Figure 3a and b. We use these values to compute Akhiezer dissipation using eq 1 and compare with NEMD results.

The NEMD simulation for the empty CNT (case I) is carried out in the frequency range 2.5 to 16 GHz at 2% strain amplitude. The highest frequency considered is much less than the fundamental frequency of axial vibration of the CNT which is ~1 THz. This ensures strain uniformity. Figure 3c shows the dissipation response for the empty CNT case. Plugging in the γ_i's and τ_i's into eq 1, dissipation is calculated and is found to compare well with the NEMD results. The comparison is shown in Figure 3c. This ascertains that the principle behind intrinsic dissipation, D_{int}^{ν} is Akhiezer mechanism. One should note that each term in the dissipation expression (eq 1) has a Lorentzian form which is a function of the metric $\Omega\tau_i$. The value of the metric governs the frequency dependence of dissipation by each phonon. For any phonon mode i, its dissipation contribution is maximum when $\Omega\tau_i \approx 1$. Also, in the case of empty CNT in vacuum, energy relaxation of a phonon takes place due to interactions with other phonons in the CNT.

Next, we address how fluid dissipates energy during axial excitation of the CNT filled with Ar. The driven motion of the resonator generates an oscillating flow field in the fluid. Since fluid is a viscous medium, it dissipates energy during the flow. The dissipated energy can be calculated from the work done by the resonator during its axial motion against the hydrodynamic force.[40,41] The idea is described in this section and is extended using linear response theory to formulate fluid dissipation in terms of equilibrium fluctuations of an observable computed using the hydrodynamic force. We also validate the formulation with NEMD results.

Fluid Dissipation. The macroscopic axial motion (along the z direction) of any wall atom, j, during the process of uniform axial straining can be expressed as $w_j(t) = z_j^0 \epsilon(t)$, where z_j^0 is the mean z coordinate of the wall atom. Due to wall−fluid interaction, the wall atoms experience a hydrodynamic force during the excitation process, which can be represented by $F_j(t)$. This leads to a change in energy of the system, E_{sys} with time which can be written as

$$\left.\frac{\partial E_{\text{sys}}}{\partial t}\right|_{\text{flu}} = -\left\langle \sum_j \dot{w}_j(t) F_j(t) \right\rangle_{\text{neq}} \tag{2}$$

Since hydrodynamic force from the fluid is responsible for the change in energy, the subscript "flu" is used. Also, the term on the right is regarded as an ensemble average during the excitation process, which is a nonequilibrium ("neq") condition. This term can be manipulated and expressed as a product of an explicitly time-dependent function, $\dot{\epsilon}(t)$, and an observable, $W_f(t)$, as

$$\left.\frac{\partial E_{\text{sys}}}{\partial t}\right|_{\text{flu}} = -\langle W_f(t)\rangle_{\text{neq}} \dot{\epsilon}(t) \tag{3}$$

where $\langle W_f(t)\rangle_{\text{neq}} = \langle \sum_j z_j^0 F_j(t)\rangle_{\text{neq}}$. $\langle W_f(t)\rangle_{\text{neq}}$ is, in general, dependent on the excitation frequency. Computing $\langle W_f(t)\rangle_{\text{neq}}$ directly from NEMD simulation for each excitation frequency is expensive. A more efficient approach for estimating $\langle W_f(t)\rangle_{\text{neq}}$ is to use linear response theory (LRT).[42] According to LRT, the response of a system initially at thermal equilibrium, to a small perturbation by any external parameter can be predicted from the thermal fluctuations of the system at equilibrium. For instance, ensemble average of any physical observable B of the system at the perturbed nonequilibrium state can be expressed as the convolution of the external parameter, $\lambda(t)$ and

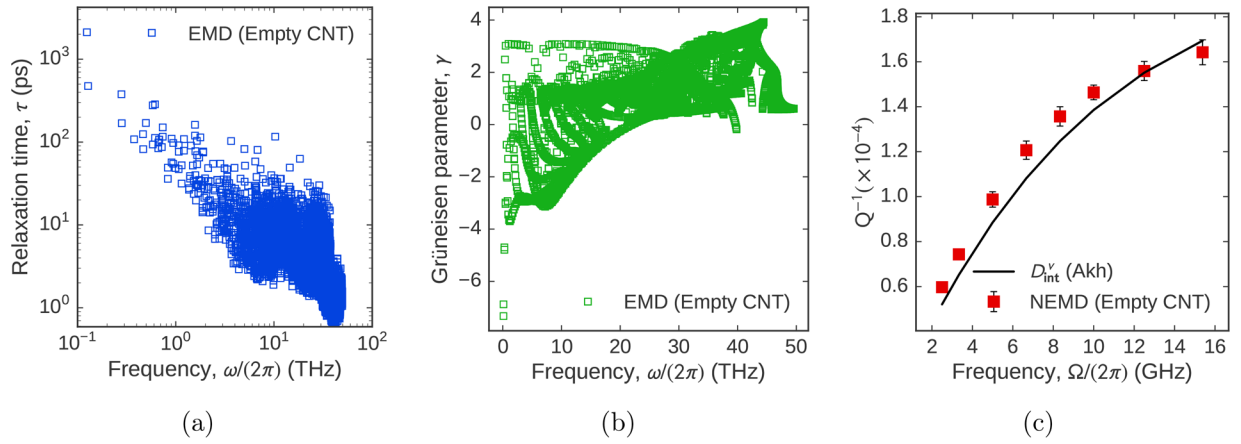

Figure 3. For the empty CNT in vacuum (Figure 1c), (a) relaxation time and (b) Grüneisen parameter vs frequency of the phonons, (c) scaling of the inverse quality factor, Q^{-1} with frequency of axial excitation, Ω where the red squares with error bars are the data points obtained from NEMD simulations and the black solid line is the estimate from Akhiezer dissipation formulation (eq 1).

DOI: 10.1021/acsnano.7b06469
ACS Nano 2018, 12, 368−377

an "after-effect" function, χ_{AB}, as[43,44]

$$\langle \Delta B(t)\rangle = \int_{-\infty}^{\infty} dt' \chi_{AB}(t-t')\lambda(t') \tag{4}$$

Here, $\langle \Delta B(t)\rangle = \langle B(t)\rangle_{neq} - \langle B(t)\rangle_{eq}$ where $\langle . \rangle_{neq}$ and $\langle . \rangle_{eq}$ denote the ensemble average taken in the nonequilibrium and equilibrium state, respectively. A is the internal variable conjugate to λ and is related to the Hamiltonian of the system is $H(t) = H_0 - \lambda(t)A$. Since the response is causal, χ_{AB} is nonzero only when $t > t'$. χ_{AB} can be expressed in terms of time correlation of the equilibrium fluctuations in A and B as

$$\begin{aligned} \chi_{AB}(t) &= -\beta \frac{d}{dt}\langle \delta A(0)\delta B(t)\rangle_{eq} \quad \text{for } t > 0 \\ &= 0 \quad \text{for } t \le 0 \end{aligned} \tag{5}$$

Here, $\beta = (k_B T)^{-1}$. $\delta A = A - \langle A\rangle_{eq}$ and $\delta B = B - \langle B\rangle_{eq}$ are thermal fluctuations in variables A and B, respectively.

In the present case of the resonator system, the external parameter $\lambda(t)$ is the time-dependent strain field $\epsilon(t)$ and its conjugate internal variable A is $W_f = \sum_j z_j^0 F_j$. The observable of interest B is also W_f. Thus, the response of $\langle \Delta W_f(t)\rangle$ to the perturbation $\epsilon(t)$ can be written as

$$\langle \Delta W_f(t)\rangle = \int_{-\infty}^{t} dt' \chi_{W_f W_f}(t-t')\epsilon(t') \tag{6}$$

where $\chi_{W_f W_f}$ is obtained by substituting A and B with W_f in eq 5. For a periodic strain field $\epsilon(t)$ of form $\epsilon_0 \sin(\Omega t)$, eq 3 along with eq 6 can be used to calculate the fluid dissipation over a time period T $(=2\pi/\Omega)$ as

$$\begin{aligned} D_{flu} &= \int_0^T dt \left.\frac{\partial E_{sys}}{\partial t}\right|_{flu} \\ &= \pi\beta\Omega\epsilon_0^2 \int_0^{\infty} dt \langle \delta W_f(0)\delta W_f(t)\rangle_{eq} \cos(\Omega t) \\ &\equiv \pi\beta\Omega\epsilon_0^2 \int_0^{\infty} dt \left\langle \left(\sum_j z_j^0 \delta F_j(0)\right)\left(\sum_j z_j^0 \delta F_j(t)\right)\right\rangle_{eq} \cos(\Omega t) \end{aligned} \tag{7}$$

From here on, we denote $\left\langle \left(\sum_j z_j^0 \delta F_j(0)\right)\left(\sum_j z_j^0 \delta F_j(t)\right)\right\rangle_{eq}$ by $\mathcal{K}_{W_f W_f}(t)$. To demonstrate the validity of this formulation, we consider the case of CNT with thermal motions frozen (case II, shown in Figure 1d). Using the hydrodynamic force on the wall atoms, F_j from EMD simulations, we calculate W_f. We, then, compute $\mathcal{K}_{W_f W_f}(t)$ and average it over 10 ensembles. The plot of $\mathcal{K}_{W_f W_f}(t)$ for different densities of filled Ar is shown in Figure 4a. Using eq 7, $\mathcal{K}_{W_f W_f}(t)$ can be used to calculate D_{flu} at each density for different excitation frequencies. To estimate D_{flu} using NEMD simulation, we artificially impose the macroscopic motion of the wall atoms as $w_j(t) = z_j^0 \epsilon_0 \sin(\Omega t)$. Since the thermal motion of all the wall atoms is completely frozen, the dissipation in the system is solely fluid dissipation. For ρ^*=0.34, the frequency response of the dissipation from NEMD simulation is shown in Figure 4b. It is in good agreement with D_{flu} estimated from eq 7 using LRT. For the density scaling of fluid dissipation, the LRT estimates are again found to agree well with NEMD results for different excitation frequencies as shown in Figure 4c. From these results, we can conclude that eq 7, obtained using LRT, provides a good estimate of fluid dissipation.

The magnitude of fluid dissipation (Figure 4b) is found to be of the same order as the intrinsic dissipation of the resonator in vacuum (Figure 3c). The comparatively low fluid dissipation can be a consequence of the confinement of the fluid inside the resonator. Previous experimental studies[18−20] on microfluidic channel based resonators have demonstrated a drastic reduction in fluid dissipation due to fluid confinement compared to a fluid exterior case. However, the extremely low magnitude of fluid dissipation in the present case could involve additional effects of nanoscale confinement like interfacial slip, anisotropic viscosity,[45] etc. These effects are incorporated in the hydrodynamic response of the fluid obtained directly from MD. At low excitation frequencies, *i.e.*, 5 and 12 GHz, the fluid dissipation increases with the increase in density. At higher excitation frequency, the fluid dissipation scales nonmonotonically with density. The difference in scaling behavior at low and high frequency regimes can be attributed to the finite time scale of relaxation[25] of the response of the hydrodynamic force (as can be seen from Figure 4a). Similar effects have been interpreted previously in terms of frequency dependent slip lengths.[46] In general, increase in density leads to increase in viscosity in the hydrodynamic limit $(\Omega \to 0)$. This explains the

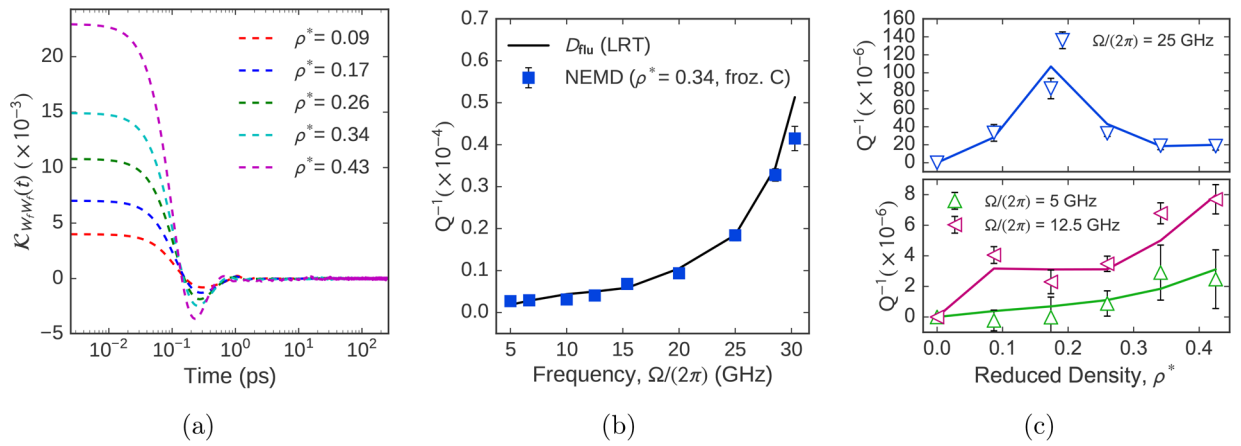

Figure 4. For the fluid coupled resonator system with frozen carbon atoms (Figure 1d), (a) $\mathcal{K}_{W_f W_f}(t)$ vs time at different densities of filled Ar obtained from equilibrium molecular dynamics (EMD) simulations, (b) scaling of inverse quality factor, Q^{-1} with frequency of axial excitation, Ω at reduced density, ρ^*= 0.34, (c) scaling of inverse quality factor with density of filled argon at different excitation frequencies. In (b) and (c), the markers with error bars are the data points obtained from NEMD simulations and the solid lines are the estimates from fluid dissipation formulation (eq 7).

DOI: 10.1021/acsnano.7b06469
ACS Nano 2018, 12, 368−377

increase in fluid dissipation with density at lower excitation frequencies. But, at higher frequencies, the time scale of the response of the fluid becomes comparable to the period of excitation and this could manifest in a different scaling of viscous dissipation.

Now we turn to the coupled system (with both CNT and Ar at 300 K) and look at the total dissipation in terms of fluid and Akhiezer contribution. In the process, we elucidate the effect of phonon-fluid interaction to each dissipation mechanism.

Phonon-Fluid Interaction. To estimate the fluid dissipation contribution for the coupled system, we first compute $\mathcal{K}_{W_fW_f}(t)$. The plot of $\mathcal{K}_{W_fW_f}(t)$ with time at different densities of filled Ar is shown in Figure 5b. The initial value, *i.e.*, $\mathcal{K}_{W_fW_f}(0)$ at different densities is found to differ slightly from case II. It should be noted that in case of the coupled system, thermal vibration of the carbon atoms in the CNT is present which was frozen in case II. The coherent motion of the CNT atoms (phonons) affect the dynamics of adjacent fluid atoms. This effect is captured while computing the scaled correlation of the forces F_j on the wall atoms using eq 3 and accounts for the difference in $\mathcal{K}_{W_fW_f}(0)$.

The intrinsic dissipation due to Akhiezer mechanism depends on two phonon parameters: γ and τ. Out of these two parameters, τ is more susceptible to fluidic interaction. In the absence of fluid, the phonons in the CNT share energy only with other phonons via phonon−phonon scattering. Fluid presents an additional channel to the phonons to share their energy via phonon-fluid scattering.[47] As a result, any perturbation in phonon energies relaxes faster in the presence of fluid coupling. This is revealed by recalculating the phonon relaxation times, τ_i's for the fluid coupled resonator system. To do so, we use the atomic trajectories of the CNT obtained from EMD simulation of the coupled system. The trajectories incorporate the effect of nonbonded interactions from the fluid atoms. These trajectories are used to calculate the energy fluctuation of each phonon mode. τ_i for each mode calculated from autocorrelation of these fluctuations is shown in Figure 5a. This corresponds to the case with $\rho^* = 0.34$. When compared to τ_i's of an empty CNT, it is found that there is a significant reduction in relaxation times of low-frequency phonons. Some studies have shown similar coupling of low-frequency phonons of the CNT with surrounding Ar matrix[31] and confined water.[48] The coupling manifested into faster relaxation of thermal energy of the phonons[31] and reduction in thermal conductivity,[48] respectively.

We analyze the frequency scaling of total dissipation in terms of these individual dissipation mechanisms for $\rho^* = 0.34$.

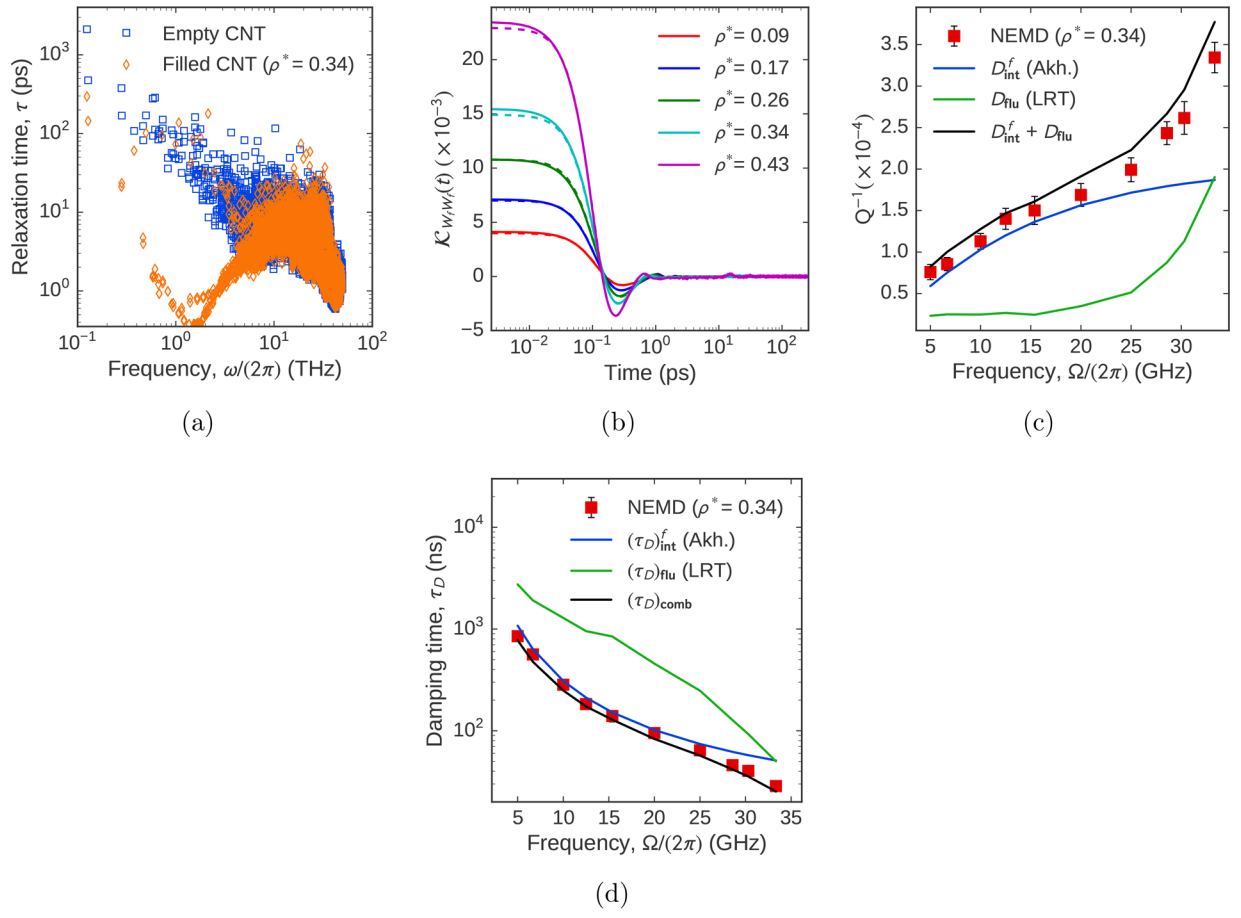

Figure 5. (a) A comparison of phonon relaxation times for the CNT filled with Ar (Figure 1a) at density, ρ^*= 0.34 with that of the empty CNT in vacuum (Figure 1c). (b) A comparison of $\mathcal{K}_{W_fW_f}(t)$ computed for the Ar filled CNT with phonons (Figure 1a) and Ar filled CNT with carbon atoms frozen (Figure 1d) shown with solid and dashed lines, respectively. (c and d) Scaling of (c) dissipation and (d) damping time in the Ar filled CNT system with the frequency of excitation, Ω. The markers with error bars are the data points for net dissipation (c) and damping time (d) obtained from NEMD simulations. The green and the blue solid lines are the intrinsic dissipation and fluid dissipation contributions, respectively in (c), and the damping time due to intrinsic and fluidic contributions, respectively in (d). The combined effect of each contribution, represented by black solid line is compared to the NEMD results. In (d), $(\tau_D)_{comb}=[(\tau_D^{-1})^f_{int}+(\tau_D^{-1})_{flu}]^{-1}$.

DOI: 10.1021/acsnano.7b06469
ACS Nano 2018, 12, 368−377

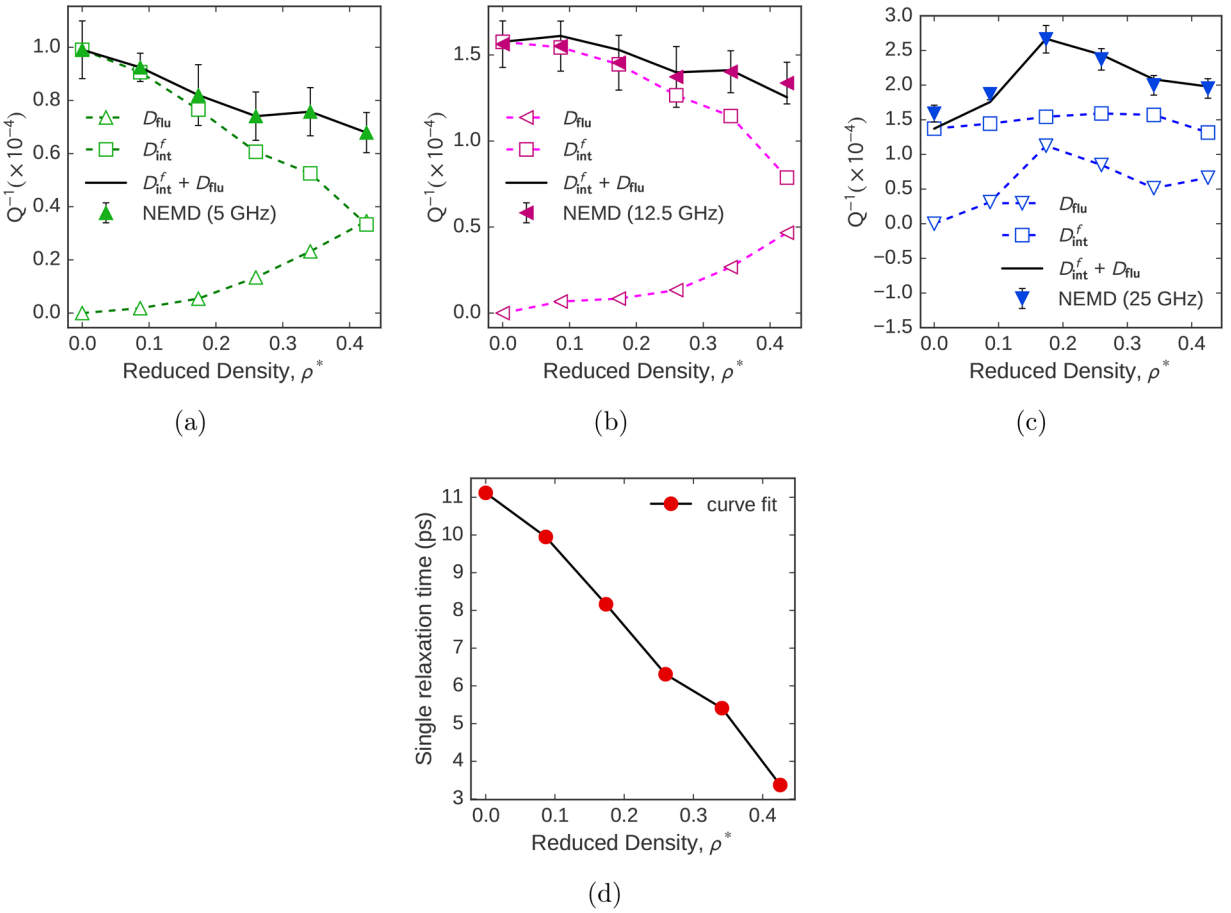

Figure 6. Scaling of dissipation with density, ρ^* in the Ar filled CNT system (Figure 1a) at (a) 5 GHz, (b) 12.5 GHz, and (c) 25 GHz excitation frequencies. The filled triangles with error bars are the data points for net dissipation obtained from NEMD simulations. The empty squares and the empty triangles show the intrinsic and the fluid dissipation contributions, respectively, to the net dissipation. (d) Under the single relaxation time approximation of Akhiezer dissipation, change in relaxation time, τ_s with the density, ρ^* of filled Ar.

Using $\mathcal{K}_{W_fW_f}(t)$ computed for $\rho^* = 0.34$ in eq 7, the fluid dissipation component is estimated as a function of excitation frequencies, Ω. To estimate the Akhiezer contribution, we plug in the τ_i for each phonon computed for the coupled system in eq 1 which gives us D^f_{int}. Figure 5c shows the net dissipation and the dissipation contribution by each component. The sum of the contributions compares well with the net dissipation of the system obtained using NEMD. Each component of dissipation will govern a decay time, τ_D, of any initial axial excitation of the system. τ_D can be defined as $\tau_D = 2Q/\Omega$. Figure 5d shows the decay time due to each dissipative component along with the decay time due to their combined effect. It can be seen from the plots in Figure 5c and d that the total dissipation in the system is primarily due to the Akhiezer mechanism at lower excitation frequencies. As we gradually move to higher excitation frequencies, fluid dissipation starts playing a role. Since Akhiezer dissipation plays a dominant role and is a function of the metric $\Omega\tau_i$, any change in the τ_i by modifying the density of filled Ar will manifest in the total dissipation in the system. In the next section, we attempt to analyze the effect of density of the confined fluid on individual dissipation mechanisms.

Density Scaling of Dissipation. We use $\mathcal{K}_{W_fW_f}(t)$ computed at different fluid densities to estimate the fluid dissipation component. The scaling of the fluid dissipation with density at three different excitation frequencies is shown in Figure 6a–c. At lower excitation frequencies, *i.e.*, 5 GHz (Figure 6a) and 12.5 GHz (Figure 6b), the fluid dissipation increases with increase in density. Whereas at 25 GHz (Figure 6c) the fluid dissipation scales nonmonotonically with density. It should be noted that though the scaling behavior of the fluid dissipation is similar to case II, the magnitude is quite different due to the difference in $\mathcal{K}_{W_fW_f}(t)$.

By subtracting fluid dissipation from the total dissipation obtained from NEMD, we can calculate the Akhiezer contribution. For the 5 GHz case, we calculate the Akhiezer contribution and fit it with single-relaxation time approximation of Akhiezer dissipation. Under this approximation, Akhiezer dissipation can be expressed[36] $D^s_{Akh} = \pi k_B T \Delta\gamma_s^2 \frac{\Omega\tau_s}{1+(\Omega\tau_s)^2}\epsilon_0^2$, where τ_s can be interpreted as time scale of collective relaxation of phonon energies. A least-squares fitting yields values of τ_s at different fluid densities. τ_s is found to decrease with increase in fluid density as shown in Figure 6d. This can be explained in terms of increase in fluidic interaction. With the increase in fluid density, the same number of phonon modes interact with increased number of fluid atoms. The increased fraction of fluidic interaction per phonon mode enables faster relaxation of their energy. The reduction of τ_s manifests itself in dependence of Akhiezer dissipation on fluid density at different frequencies. Using the values of τ_s, the Akhiezer dissipation is estimated for 12.5 and 25 GHz cases. The sum of Akhiezer and fluid contribution is found to agree well with the NEMD results for total

DOI: 10.1021/acsnano.7b06469
ACS Nano 2018, 12, 368–377

dissipation. At 5 and 12.5 GHz, fluid dissipation has a negligible contribution and Akhiezer dissipation governs the scaling of total dissipation with density. At these frequencies, Akhiezer dissipation decreases with increase in density due to a reduction in τ_s and consequently total dissipation decreases. However, at 25 GHz, Akhiezer dissipation does not change much with the reduction in τ_s. In fact, fluid dissipation has a significant contribution and its nonmonotonic scaling with density governs the scaling of total dissipation.

CONCLUSIONS

In summary, we examine the effect of phonon-fluid coupling on dissipation of a fluid coupled nanoresonator system driven at gigahertz frequencies. Our MD simulations on frequency and density scaling of total dissipation incorporate the phonon-fluid coupling effect directly. However, to analyze the consequences arising solely due to the coupling effect, we resorted to theoretical formulation of each dissipative process in the system. We identify that the total dissipation is contributed by intrinsic dissipation (D^f_{int}) governed by Akhiezer mechanism and fluid dissipation (D_{flu}). We formulate the fluid dissipation in terms of hydrodynamic force on the resonator and observe that its magnitude is either very low or comparable to the intrinsic dissipation. As experimental observations on fluidic channel based resonator[18−20] suggests, the relatively low fluid dissipation is a consequence of confining the fluid inside the CNT instead of placing it outside. Another consequence is nonmonotonic scaling of fluid dissipation with the density of the fluid, which we observe at higher excitation frequencies. Besides that, the fluid dissipation is found to increase monotonically with excitation frequency for a given density and with density for low excitation frequencies. We confirm our formulation of intrinsic dissipation due to Akhiezer mechanism by considering the case of empty CNT in vacuum. The formulation reveals that the strength of the Akhiezer dissipation depends on the metric $\Omega\tau$, where Ω is the excitation frequency and τ is the phonon relaxation time. Since τ mostly varies between 1 and 100 ps for a CNT at room temperature, Akhiezer mechanism becomes dominant at gigahertz excitations. We find these relaxation times are affected by the phonon-fluid coupling and is manifested in the Akhiezer dissipation. This leads to a change in the intrinsic dissipation of the resonator in the presence of fluid at a given density when compared with that of vacuum (D^v_{int}). This change ($\Delta D_{\text{int}}=D^f_{\text{int}}-D^v_{\text{int}}$) has been ignored in all previous studies of fluid coupled resonator systems. In our case, accounting for the change becomes particularly crucial since the order of $\Delta D_{\text{int}} \sim D^v_{\text{int}} \sim D_{\text{flu}}$. Further, we find that the phonon-fluid coupling strength and consequently the phonon relaxation times can be manipulated by changing the fluid density. We show that an important consequence of the coupling on the total dissipation is its inverse scaling with the density of the fluid at some frequencies. Although, the consequence of phonon-fluid coupling is presented, in this study, in the context of intrinsic dissipation due to Akhiezer mechanism, the coupling effect is general and extends to calculation of any material parameter that depends on phonon relaxation times, such as thermal conductivity, thermal diffusion time, etc., in the presence of interfacial fluidic interaction.

METHODS

We construct a (10,10) single-walled carbon nanotube (CNT) of length 20 nm, which corresponds to 3280 carbon atoms and a tube radius of 0.68 nm. The CNT is filled with argon (Ar) atoms at different densities. To restrict the Ar atoms inside the tube, we place a sheet of monolayer graphene of dimension 1.6 nm × 1.6 nm on each end of the CNT. The CNT and the graphene layers comprise the wall which confines the fluid composed of Ar atoms as shown in Figure 1a. The optimized Tersoff and Brenner potential[30] is used to describe the bonded interaction between the carbon (C) atoms in the CNT. Since the C atoms in the graphene sheets are kept frozen during all the simulations, their interaction is not relevant. Even the interaction between the graphene sheets and the CNT is neglected. The nonbonded interaction between the Ar atoms and the C atoms in the CNT and the graphene sheets is modeled using the two-body Lennard-Jones (LJ) potential.[31]

We use LAMMPS package[32] for all the molecular simulations. The CNT is prestretched by 5% to avoid any buckling during the axial deformation. Two rings of atoms on each end of the CNT which corresponds to 80 C atoms along with C atoms of the graphene sheets are kept frozen for all the simulations. The rest of the CNT along with the fluid defines our system (sys) whereas the frozen part acts as a clamp as shown in Figure 1a. The potential energy of the system is minimized using the conjugate-gradient method which gives the starting configuration. The atoms of the system are, then, given an initial velocity drawn from a Gaussian distribution corresponding to a temperature of 300 K. The system is evolved under canonical (NVT) ensemble using Nosé−Hoover thermostat[33,34] for 5 ns and equilibrated at 300 K.

For computing dissipation in the system, we conduct nonequilibrium molecular dynamics (NEMD) simulations. The clamps are moved apart at a particular frequency to produce a time-varying axial strain field in the structure. During the deformation process, the system is evolved under microcanonical (NVE) ensemble using Verlet integration (no thermostat). Under this consideration, any change in total energy of the system over a period of deformation is equal to the energy dissipated by the system. The NEMD simulations are carried out for 50 periods of deformation. The total energy of the system averaged over a period of deformation is found to increase linearly with the number of periods (shown in Figure 1b). A linear fit of the average energy with the number of periods is performed and from the slope of the linear fit dissipation of the system, D_{sys} is calculated. We considered 10 different ensembles of the equilibrated system to estimate the dissipation using NEMD simulations. E_{sto} is obtained using separate equilibrium simulations. Following the initial equilibration, the structure is deformed and allowed to relax for 1 ns for different values of strain. E_{sto} in the structure varies as the square of strain. Using curve fit, we obtain the constant of proportionality, which is the stiffness of the structure, k. E_{sto} at any stain amplitude, ϵ_0, can then be calculated as $1/2k\epsilon_0^2$. In all our cases, E_{sto} corresponding to 2% strain amplitude is approximately 154 eV.

Out of the two additional setups, the first setup (case I, shown in Figure 1c), which represents an isolated CNT in vacuum (v), is prepared by removing all the fluid atoms from the system. The dissipation, D^v_{int} under axial straining is calculated for this system using NEMD simulations. The second setup (case II, shown in Figure 1d) involves freezing the thermal motions in the CNT of the original system. This is implemented in MD simulations by applying zero initial velocity to the C atoms in CNT and carrying out time integration of only the Ar atoms during the simulation. In this case, the NEMD simulations are carried out, to compute dissipation, by artificially imposing a prescribed motion on the wall atoms.

We, also, carry out equilibrium molecular dynamics (EMD) simulations of these setups. The atomic trajectories and forces from the EMD simulations are used to compute different parameters of interest in the dissipation formulation. We start with a system, well equilibrated at 300 K and evolve the system under NVE ensemble for 5 ns in case of the EMD simulations. The trajectories and forces are dumped every 5 fs during the simulation. The integration time step for all the simulations is set to 0.5 fs. The time step is small enough to sufficiently resolve the highest frequency of the thermal phonons in a CNT which is approximately 60 THz.

AUTHOR INFORMATION

Corresponding Author

*aluru@illinois.edu

DOI: 10.1021/acsnano.7b06469
ACS Nano 2018, 12, 368−377

ORCID

Subhadeep De: 0000-0003-0936-1956

Notes

The authors declare no competing financial interest.

ACKNOWLEDGMENTS

We gratefully acknowledge the support by NSF under grants 1420882 and 1506619.

REFERENCES

(1) Cui, Y.; Wei, Q.; Park, H.; Lieber, C. M. Nanowire Nanosensors for Highly Sensitive and Selective Detection of Biological and Chemical Species. *Science* **2001**, *293*, 1289−1292.

(2) Patolsky, F.; Zheng, G.; Lieber, C. M. Fabrication of Silicon Nanowire Devices for Ultrasensitive, Label-Free, Real-Time Detection of Biological and Chemical Species. *Nat. Protoc.* **2006**, *1*, 1711−1724.

(3) Lassagne, B.; Garcia-Sanchez, D.; Aguasca, A.; Bachtold, A. Ultrasensitive Mass Sensing with a Nanotube Electromechanical Resonator. *Nano Lett.* **2008**, *8*, 3735−3738.

(4) Gil-Santos, E.; Ramos, D.; Martínez, J.; Fernández-Regúlez, M.; García, R.; San Paulo, Á.; Calleja, M.; Tamayo, J. Nanomechanical Mass Sensing and Stiffness Spectrometry Based on Two-Dimensional Vibrations of Resonant Nanowires. *Nat. Nanotechnol.* **2010**, *5*, 641−645.

(5) Chen, R. J.; Bangsaruntip, S.; Drouvalakis, K. A.; Kam, N. W. S.; Shim, M.; Li, Y.; Kim, W.; Utz, P. J.; Dai, H. Noncovalent Functionalization of Carbon Nanotubes for Highly Specific Electronic Biosensors. *Proc. Natl. Acad. Sci. U. S. A.* **2003**, *100*, 4984−4989.

(6) Zheng, G.; Patolsky, F.; Cui, Y.; Wang, W. U.; Lieber, C. M. Multiplexed Electrical Detection of Cancer Markers with Nanowire Sensor Arrays. *Nat. Biotechnol.* **2005**, *23*, 1294−1301.

(7) Jensen, K.; Kim, K.; Zettl, A. An Atomic-Resolution Nanomechanical Mass Sensor. *Nat. Nanotechnol.* **2008**, *3*, 533−537.

(8) Naik, A.; Hanay, M.; Hiebert, W.; Feng, X.; Roukes, M. Towards Single-Molecule Nanomechanical Mass Spectrometry. *Nat. Nanotechnol.* **2009**, *4*, 445−450.

(9) Moser, J.; Eichler, A.; Güttinger, J.; Dykman, M. I.; Bachtold, A. Nanotube Mechanical Resonators with Quality Factors of up to 5 Million. *Nat. Nanotechnol.* **2014**, *9*, 1007−1011.

(10) Tao, Y.; Boss, J.; Moores, B.; Degen, C. Single-Crystal Diamond Nanomechanical Resonators with Quality Factors Exceeding One Million. *Nat. Commun.* **2014**, *5*.510.1038/ncomms4638

(11) Eichler, A.; Moser, J.; Chaste, J.; Zdrojek, M.; Wilson-Rae, I.; Bachtold, A. Nonlinear Damping in Mechanical Resonators Made from Carbon Nanotubes and Graphene. *Nat. Nanotechnol.* **2011**, *6*, 339−342.

(12) Hanay, M.; Kelber, S.; Naik, A.; Chi, D.; Hentz, S.; Bullard, E.; Colinet, E.; Duraffourg, L.; Roukes, M. Single-Protein Nanomechanical Mass Spectrometry in Real Time. *Nat. Nanotechnol.* **2012**, *7*, 602−608.

(13) Ilic, B.; Yang, Y.; Aubin, K.; Reichenbach, R.; Krylov, S.; Craighead, H. Enumeration of DNa Molecules Bound to a Nanomechanical Oscillator. *Nano Lett.* **2005**, *5*, 925−929.

(14) Lifshitz, R.; Roukes, M. L. Thermoelastic Damping in Micro-and Nanomechanical Systems. *Phys. Rev. B: Condens. Matter Mater. Phys.* **2000**, *61*, 5600.

(15) Kiselev, A.; Iafrate, G. Phonon Dynamics and Phonon Assisted Losses in Euler-Bernoulli Nanobeams. *Phys. Rev. B: Condens. Matter Mater. Phys.* **2008**, *77*, 205436.

(16) Kunal, K.; Aluru, N. Akhiezer Damping in Nanostructures. *Phys. Rev. B: Condens. Matter Mater. Phys.* **2011**, *84*, 245450.

(17) Seoánez, C.; Guinea, F.; Neto, A. C. Surface Dissipation in Nanoelectromechanical Systems: Unified Description with the Standard Tunneling Model and Effects of Metallic Electrodes. *Phys. Rev. B: Condens. Matter Mater. Phys.* **2008**, *77*, 125107.

(18) Burg, T. P.; Godin, M.; Knudsen, S. M.; Shen, W.; Carlson, G.; Foster, J. S.; Babcock, K.; Manalis, S. R. Weighing of Biomolecules, Single Cells and Single Nanoparticles in Fluid. *Nature* **2007**, *446*, 1066−1069.

(19) Barton, R. A.; Ilic, B.; Verbridge, S. S.; Cipriany, B. R.; Parpia, J. M.; Craighead, H. G. Fabrication of a Nanomechanical Mass Sensor Containing a Nanofluidic Channel. *Nano Lett.* **2010**, *10*, 2058−2063.

(20) Lee, J.; Shen, W.; Payer, K.; Burg, T. P.; Manalis, S. R. Toward Attogram Mass Measurements in Solution with Suspended Nanochannel Resonators. *Nano Lett.* **2010**, *10*, 2537−2542.

(21) De, S. K.; Aluru, N. Theory of Thermoelastic Damping in Electrostatically Actuated Microstructures. *Phys. Rev. B: Condens. Matter Mater. Phys.* **2006**, *74*, 144305.

(22) De, S.; Kunal, K.; Aluru, N. Nonlinear Intrinsic Dissipation in Single Layer MoS_2 Resonators. *RSC Adv.* **2017**, *7*, 6403−6410.

(23) Iyer, S. S.; Candler, R. N. Mode-and Direction-Dependent Mechanical Energy Dissipation in Single-Crystal Resonators Due to Anharmonic Phonon-Phonon Scattering. *Phys. Rev. Appl.* **2016**, *5*, 034002.

(24) Yakhot, V.; Colosqui, C. Stokes' Second Flow Problem in a High-Frequency Limit: Application to Nanomechanical Resonators. *J. Fluid Mech.* **2007**, *586*, 249−258.

(25) Pelton, M.; Chakraborty, D.; Malachosky, E.; Guyot-Sionnest, P.; Sader, J. E. Viscoelastic Flows in Simple Liquids Generated by Vibrating Nanostructures. *Phys. Rev. Lett.* **2013**, *111*, 244502.

(26) Kara, V.; Sohn, Y.-I.; Atikian, H.; Yakhot, V.; Loncar, M.; Ekinci, K. L. Nanofluidics of Single-Crystal Diamond Nanomechanical Resonators. *Nano Lett.* **2015**, *15*, 8070−8076.

(27) Burg, T. P.; Sader, J. E.; Manalis, S. R. Nonmonotonic Energy Dissipation in Microfluidic Resonators. *Phys. Rev. Lett.* **2009**, *102*, 228103.

(28) Ruijgrok, P. V.; Zijlstra, P.; Tchebotareva, A. L.; Orrit, M. Damping of Acoustic Vibrations of Single Gold Nanoparticles Optically Trapped in Water. *Nano Lett.* **2012**, *12*, 1063−1069.

(29) Yu, K.; Zijlstra, P.; Sader, J. E.; Xu, Q.-H.; Orrit, M. Damping of Acoustic Vibrations of Immobilized Single Gold Nanorods in Different Environments. *Nano Lett.* **2013**, *13*, 2710−2716.

(30) Lindsay, L.; Broido, D. Optimized Tersoff and Brenner Empirical Potential Parameters for Lattice Dynamics and Phonon Thermal Transport in Carbon Nanotubes and Graphene. *Phys. Rev. B: Condens. Matter Mater. Phys.* **2010**, *81*, 205441.

(31) Carlborg, C. F.; Shiomi, J.; Maruyama, S. Thermal Boundary Resistance Between Single-Walled Carbon Nanotubes and Surrounding Matrices. *Phys. Rev. B: Condens. Matter Mater. Phys.* **2008**, *78*, 205406.

(32) Plimpton, S.; Crozier, P.; Thompson, A. *LAMMPS-Large-Scale Atomic/molecular Massively Parallel Simulator*; 2007, Vol. *18*.

(33) Hoover, W. G.; Ladd, A. J.; Moran, B. High-Strain-Rate Plastic Flow Studied Via Nonequilibrium Molecular Dynamics. *Phys. Rev. Lett.* **1982**, *48*, 1818.

(34) Nosé, S. A. Unified Formulation of the Constant Temperature Molecular Dynamics Methods. *J. Chem. Phys.* **1984**, *81*, 511−519.

(35) Kulsrud, R. M. Adiabatic Invariant of the Harmonic Oscillator. *Phys. Rev.* **1957**, *106*, 205.

(36) De, S.; Kunal, K.; Aluru, N. Mixed Role of Surface on Intrinsic Losses in Silicon Nanostructures. *J. Appl. Phys.* **2016**, *119*, 114304.

(37) McGaughey, A. J.; Kaviany, M. Quantitative Validation of the Boltzmann Transport Equation Phonon Thermal Conductivity Model Under the Single-Mode Relaxation Time Approximation. *Phys. Rev. B: Condens. Matter Mater. Phys.* **2004**, *69*, 094303.

(38) Tang, Z.; Zhao, H.; Li, G.; Aluru, N. Finite-Temperature Quasicontinuum Method for Multiscale Analysis of Silicon Nanostructures. *Phys. Rev. B: Condens. Matter Mater. Phys.* **2006**, *74*, 064110.

(39) Ladd, A. J.; Moran, B.; Hoover, W. G. Lattice Thermal Conductivity: A Comparison of Molecular Dynamics and Anharmonic Lattice Dynamics. *Phys. Rev. B: Condens. Matter Mater. Phys.* **1986**, *34*, 5058.

(40) Sader, J. E. Frequency Response of Cantilever Beams Immersed in Viscous Fluids with Applications to the Atomic Force Microscope. *J. Appl. Phys.* **1998**, *84*, 64−76.

DOI: 10.1021/acsnano.7b06469
ACS Nano 2018, 12, 368−377

(41) Paul, M.; Cross, M. Stochastic Dynamics of Nanoscale Mechanical Oscillators Immersed in a Viscous Fluid. *Phys. Rev. Lett.* **2004**, *92*, 235501.
(42) Kubo, R. The Fluctuation-Dissipation Theorem. *Rep. Prog. Phys.* **1966**, *29*, 255.
(43) Frenkel, D.; Smit, B. *Understanding Mol. Simul.: From Algorithms to Applications*; Academic Press, 2001; Vol. *1*.
(44) Huang, K.; Szlufarska, I. Green−Kubo Relation for Friction at Liquid-Solid Interfaces. *Phys. Rev. E* **2014**, *89*, 032119.
(45) Bhadauria, R.; Sanghi, T.; Aluru, N. Interfacial Friction Based Quasi-Continuum Hydrodynamical Model for Nanofluidic Transport of Water. *J. Chem. Phys.* **2015**, *143*, 174702.
(46) Huang, K.; Szlufarska, I. Friction and Slip at the Solid/liquid Interface in Vibrational Systems. *Langmuir* **2012**, *28*, 17302−17312.
(47) Thomas, J. A.; Turney, J. E.; Iutzi, R. M.; Amon, C. H.; McGaughey, A. J. Predicting Phonon Dispersion Relations and Lifetimes from the Spectral Energy Density. *Phys. Rev. B: Condens. Matter Mater. Phys.* **2010**, *81*, 081411.
(48) Thomas, J. A.; Iutzi, R. M.; McGaughey, A. J. Thermal Conductivity and Phonon Transport in Empty and Water-Filled Carbon Nanotubes. *Phys. Rev. B: Condens. Matter Mater. Phys.* **2010**, *81*, 045413.

DOI: 10.1021/acsnano.7b06469
ACS Nano 2018, 12, 368−377